

# Spin dynamics and criteria for onset of exchange bias in superspin glass Fe/ $\gamma$ -Fe<sub>2</sub>O<sub>3</sub> core-shell nanoparticles

Sayan Chandra,<sup>1</sup> H. Khurshid,<sup>1,2</sup> Wanfeng Li,<sup>2</sup> G. C. Hadjipanayis,<sup>2</sup> M. H. Phan,<sup>1</sup> and H. Srikanth<sup>1</sup>

<sup>1</sup>*Department of Physics, University of South Florida, Tampa, Florida 33620, USA*

<sup>2</sup>*Department of Physics and Astronomy, University of Delaware, Newark, Delaware 19711, USA*

(Received 6 May 2012; revised manuscript received 2 July 2012; published 25 July 2012)

A detailed study is presented on Fe/ $\gamma$ -Fe<sub>2</sub>O<sub>3</sub> core-shell structured nanoparticles (mean size  $\sim$ 10 nm) to understand the spin dynamics of the core and shell independently and their role in triggering exchange bias (EB) phenomena. The particle dynamics critically slow down at  $T_g \sim$  68 K, below which they exhibit memory effect in field-cooled and zero-field-cooled protocols associated with a superspin glass state. The field dependence of mean blocking temperature fits the de Almeida-Thouless line and shows two different linear responses in the low and high field regimes corresponding to the core and shell, respectively. We show that the energy barrier distribution estimated from the temperature decay of isothermal remanent magnetization shows two maxima that mark the freezing temperatures of the core ( $T_{f-cr} \sim$  48 K) and shell ( $T_{f-sh} \sim$  21 K). Last, hysteresis measurements after field cooling reveal strong EB indicated by a loop shift associated with unidirectional anisotropy. The onset of EB is at 35 K when the ferromagnetic core is frozen and the moments in the ferrimagnetic shell begin to block, resulting in enhanced exchange coupling.

DOI: [10.1103/PhysRevB.86.014426](https://doi.org/10.1103/PhysRevB.86.014426)

PACS number(s): 75.75.Jn, 75.78.-n

## I. INTRODUCTION

The phenomenon of exchange bias (EB) has generated a lot of research interest over the past five decades.<sup>1-7</sup> EB has been reported in thin films with a conventional ferromagnet (FM)-antiferromagnet (AFM) interface<sup>8</sup> and in other magnetic nanostructures having ferrimagnetic (FIM) domains,<sup>9</sup> spin glasses,<sup>10</sup> or surface spin disorder.<sup>11</sup> In the case of thin films, the origin of EB is well understood and is attributed to the unidirectional anisotropy developed at the FM-AFM interface due to pinning of magnetic moments. Recent experiments have also demonstrated EB in the case of samples having a FM layer in contact with a spin glass layer;<sup>12,13</sup> layered nanoparticle/ferromagnetic structures where various models have been suggested to explain the origin of EB.<sup>14</sup> Core-shell nanoparticles with a conventional FM (core)/AFM (shell) and, more recently, “inverted” AFM (core)/FM (shell) have also been studied and the general consensus to explain EB is the freezing of interfacial spins or the growth of droplets with uncompensated spins.<sup>15-17</sup>

Usually, core-shell nanoparticles are composed of different materials. Hence, we can say that the effective anisotropy, lattice strain, number of uncompensated spins, etc., for the materials making up the core and shell differ, which, in turn, implies that these two materials may have separate responses to change in temperature and magnetic field. So a very fundamental and important question emerges: Can the dynamic and static response of the core and shell be identified separately? While several research efforts have been devoted in understanding the role of interfacial spins in nanoparticles that exhibit EB, a clear understanding of the spin dynamics of the core and shell and their impact on EB remains to be investigated.

In this paper, we have systematically demonstrated that it is possible to identify the individual responses of the core and shell. The system in the present study is  $\sim$ 10 nm Fe/ $\gamma$ -Fe<sub>2</sub>O<sub>3</sub> nanoparticles. We have shown that the nanoparticles collectively behave like a superspin glass and

exhibit distinguishably different magnetic responses of the core and shell. Our findings emphasize that by understanding the magnetic state of core and shell and their interdependence at the onset of EB, it may be possible to appropriately select different materials for core and shell to enhance and suitably tailor EB for applications.

## II. EXPERIMENT

The core-shell structured nanoparticles were prepared by use of high-temperature reduction of iron pentacarbonyl in octadecene in the presence of oleylamine (OY) and trioctyl phosphine (TOP), details of which have been published.<sup>18</sup> Briefly, OY and TOP (molar ratio 1:1) were dissolved in octadecene in a three-neck flask and heated in an airtight atmosphere while continuously purging with Ar + 5% H<sub>2</sub> to get rid of any free oxygen dissolved in the solvent and surfactants. Fe(CO)<sub>5</sub> was injected at 220°C and refluxed for 1 h to yield a dark solution. The nanoparticles were precipitated and extracted by adding absolute ethanol solution followed by centrifuging. The black powder obtained on drying was tightly packed on Kapton tape.

The structural and microstructural studies were performed using JEOL JEM 3010 FX transmission electron microscopy (TEM). The magnetic properties were carried out using a Quantum Design Physical Properties Measurement System (PPMS) with a vibrating sample magnetometer (VSM) option over a temperature range of 5 K to 300 K and applied fields up to 50 kOe.

## III. RESULTS AND DISCUSSION

Figure 1(a) shows a conventional bright-field TEM image of these nanoparticles along with a selected area diffraction pattern in the inset. The average size of the nanoparticles is determined to be  $9.8 \pm 0.7$  nm. Contrast variation at the interface clearly suggests a core and shell morphology in these

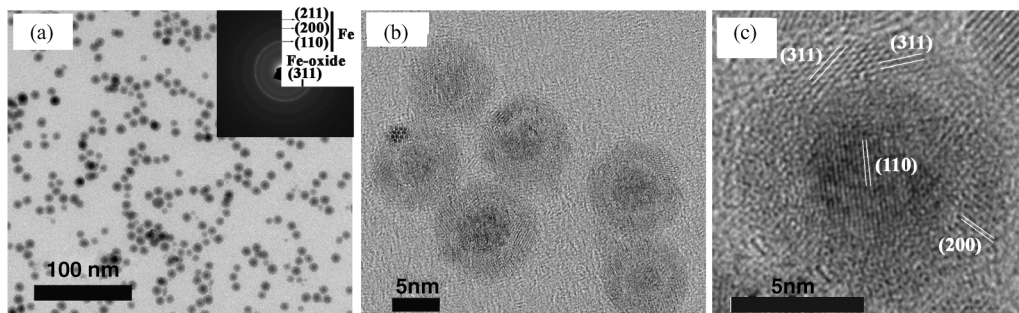


FIG. 1. Bright field (a) TEM and [(b) and (c)] HRTEM images of Fe/ $\gamma$ -Fe<sub>2</sub>O<sub>3</sub> core-shell nanoparticles. [Inset (a)] Selected area diffraction pattern.

nanoparticles. HRTEM images [Figs. 1(b) and 1(c)] reveal the crystalline structure of both core and shell, with the lattice spacing of the core and shell corresponding to the (110) planes of bcc iron and (311) planes of fcc iron oxide, respectively. The Fe core is single crystalline; however, the shell of  $\gamma$ -Fe<sub>2</sub>O<sub>3</sub> is composed of small crystallites which are oriented randomly.<sup>19</sup> In the inset of Fig. 1(a), the selected area diffraction pattern is indexed to bcc iron and fcc iron oxide. Since the particles lying on the TEM grid have no particular orientation with respect to the incident electron beam (unlike the case of thin films), the electron diffraction pattern for single crystalline core contains (211), (200), and (110) peaks.<sup>18</sup>

The nanoparticles have been tightly packed to avoid any physical motion relative to each other. Due to this tight packing, it can be safely concluded that adjacent nanoparticles touch each other with the presence of surfactant layers between them. Hence, the distance between the centers of two adjacent nanoparticles is estimated to be about 10 nm. Figure 2 presents the temperature variation in magnetization ( $M$ ) measured in 50 Oe under the zero-field-cooled (ZFC), field-cool warming (FCW), and field-cooled cooling (FCC) protocols. During the FCC and FCW measurements, the sample was cooled under an applied field of 50 Oe. The ZFC curve shows a

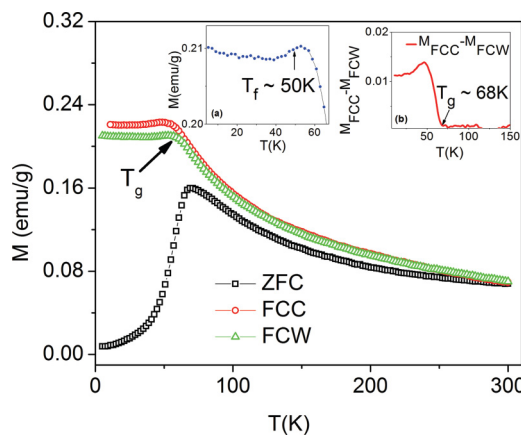


FIG. 2. (Color online) Temperature dependence of magnetization for zero-field cooling (ZFC), field cool cooling (FCC), and field cool warming (FCW). [Inset (a)] The dip in  $M_{FCW}$  is associated with onset of spin freezing ( $T_f \sim 50$  K) and (b) shows the difference ( $M_{FCC} - M_{FCW}$ ) plotted against temperature, where a sharp rise ( $T_g \sim 68$  K) marks the onset of thermal hysteresis.

conventional peak ( $T_{P-ZFC} \sim 69$  K), which has been reported in many superparamagnetic (SPM) and superspin glass (SSG) systems that are ferromagnetic in the ground state.<sup>20–22</sup> The peak in ZFC curve for monodispersed, noninteracting particles is called the blocking temperature ( $T_B$ ) and is found to occur when the thermal energy ( $k_B T$ ) is comparable to the activation energy ( $\Delta E_A = KV$ ).<sup>23</sup> However, the scenario differs markedly for interacting particles with finite-size distribution. Recent experiments have shown an increase in temperature along with broadening of the peak of ZFC curve due to enhanced interactions in the nanoparticles.<sup>24</sup> In the present case, there exists irreversibility in the ZFC and FCW curves even at room temperature, which suggests the presence of interparticle interactions or some particles in the blocked state. Due to the core-shell structure, the nature of interaction and, hence, the energy barrier is largely controlled by the relative strength of exchange anisotropy, dipole-dipole interaction, surface spin disorder, and so on. Hence, the peak ( $T_{P-ZFC}$ ) cannot be termed as the true blocking temperature of the system. Another method for determining the mean blocking temperature ( $T_B$ ) has been adopted which is discussed later. In the FCW curve, a decrease in magnetization is observed with lowering the temperature below  $\sim 50$  K as shown in the inset of Fig. 2(a). It has been reported earlier that the FCW magnetization monotonically increases with decreasing temperature for SPMs, while it tends to saturate to a constant value or even decrease with decreasing temperature for SSGs.<sup>20</sup> This feature in the FCW curve gives us a first indication that the nanoparticles show a collective glassy behavior at low temperature. There also exists a thermal hysteresis in the FCW and FCC curves below  $\sim 68$  K. The onset of thermal hysteresis is marked by a sharp rise ( $\sim T_g$ ) in  $M_{FCC} - M_{FCW}$  as shown in Fig. 2(b). Such thermal hysteresis has been reported in different systems and may occur due to various phenomena such as kinetic arrest<sup>25</sup> or phase transition of first order<sup>26</sup> or due to the presence of any thermal memory in the sample which is strongly influenced by the starting state of the system.<sup>27</sup> In our sample, which constitutes Fe(core)/ $\gamma$ -Fe<sub>2</sub>O<sub>3</sub>(shell), no such kinetic arrest or first-order transition is known for either material in that temperature range and, hence, they can be safely ruled out as reasons for thermal hysteresis. This indicates that one of the reasons for thermal hysteresis can be a cooperative effect in the system which also has a thermal memory. The above-mentioned features raise an important question about the strength and dynamics of interactions in the nanoparticles.

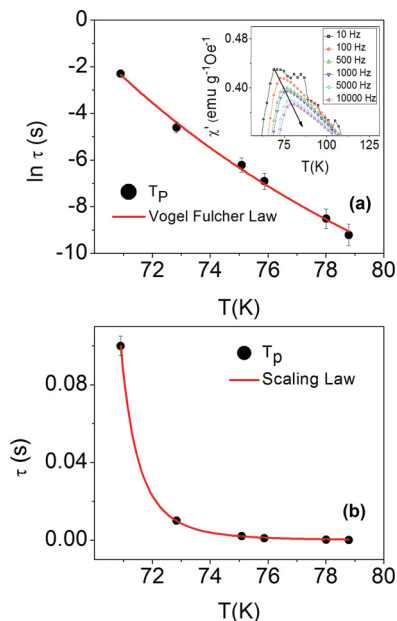


FIG. 3. (Color online) The best fit of the relaxation times ( $\tau$ ) to (a) the Vogel-Fulcher law and (b) the scaling law. (Inset) The frequency dependence of the peak temperature ( $T_p$ ) in  $\chi'$ .

To probe the spin dynamics of these nanoparticles, ac susceptibility measurements were systematically performed on the sample by applying an ac magnetic field of 10 Oe within the frequency ( $f$ ) range of 10 Hz to 10 kHz. An ensemble of interacting particles can dominate over single-particle blocking that may lead to a collective freezing. By changing the frequency, we are deliberately changing the probe time ( $\tau = 1/f$ ) which allows us to probe the relaxation of particles in different time windows. In the inset of Fig. 3(a), the frequency dependence of the real part of ac susceptibility ( $\chi'$ ) is shown. The peak temperature ( $T_p$ ) shifts to higher values as frequency increases, which is consistent with other reports.<sup>9,10</sup> A systematic investigation of the evolution of peak shift in  $\chi'$  is carried out. The peak shift in  $\chi'$  can be quantified by Eq. (1) and it is empirically known that for SPM systems,  $\Gamma$  ranges from 0.1 to 0.13, whereas, for SSG systems,<sup>28</sup>  $\Gamma < 0.06$ . For our system,  $\Gamma$  is estimated to be 0.044 which suggests that our nanoparticles may be SSG type,

$$\Gamma = \frac{\Delta T_p}{T_p \Delta(\log \omega)}. \quad (1)$$

An attempt to fit to Neel-Arrhenius (NA) law yielded unphysical results as expected. This clearly indicates that the dynamics of these nanoparticles cannot be explained with a noninteracting particle model. Thus, we extended our analysis to the Vogel-Fulcher (VF) model which takes into account weak interparticle interactions. According to the VF model, the relaxation time of an ensemble of weakly interacting nanoparticles follows Eq. (2),

$$\tau = \tau_o^{\text{VF}} \exp\left[\frac{E_a}{k_B(T - T_o)}\right]. \quad (2)$$

Here,  $E_a$  is the anisotropy energy barrier or the activation energy (KV) and  $\tau_o^{\text{VF}}$  is the relaxation time of individual

nanoparticle. The term  $T_o$  is the characteristic temperature which gives a qualitative measure of the interparticle interaction energy. The obtained fitted [Fig. 3(a)] parameters have reasonable values of  $E_a/k_B = 571$  K,  $\tau_o^{\text{VF}} = 6.9 \times 10^{-13}$  s, and  $T_o = 48$  K. This successful fit confirms the presence of weak interactions in the nanoparticles that undergo collective freezing at  $T_o \sim 48$  K, henceforth referred to as the freezing temperature ( $T_f$ ). This is in good agreement with the low-temperature feature seen in the FCW curve [Fig. 2, inset (a)]. For SPM particles,<sup>23</sup> the relaxation time  $\tau_o^{\text{VF}}$  is in the range  $10^{-8}$  to  $10^{-13}$  s. The fact that these nanoparticles fall in this range ( $\sim 10^{-13}$  s) indicates that they individually relax like SPM particles above the blocking temperature; however, in order to understand their collective behavior, the peak temperatures  $T_p$  is fitted to a critical power law (3)

$$\tau = \tau_o^{\text{SC}} \exp\left[\frac{T}{T_g} - 1\right]^{-z\nu}, \quad (3)$$

where  $T_g$  is the static spin glass temperature which marks the onset of critical slowing and collective glassy behavior;  $z\nu$  is the dynamical critical exponent which is related to the correlation length  $\xi$  that diverges at  $T_g$ . The use of such phenomenological activation law is usually done for cluster glass magnetic systems, especially SSG.<sup>29</sup> It is known from literature that for a SSG system,<sup>29-31</sup> the value of  $\tau_o^{\text{SC}}$  ranges between  $10^{-6}$  to  $10^{-9}$  s. The obtained fit parameters for our nanoparticles are  $\tau_o^{\text{SC}} = 2.8 \times 10^{-7}$  s,  $T_g = 68$  K, and  $z\nu = 3.8$ . The value of  $z\nu$  is very close to that calculated for 3D Ising model<sup>30</sup> and the value of  $\tau_o^{\text{SC}}$  further strengthens the case for SSG type of behavior. It is to be noted here that the values of  $\tau_o^{\text{VF}}$  obtained from VF model and scaling law differ; in case of the VF model,  $\tau_o^{\text{VF}}$  represents the noncritical flip time for individual particles, whereas from the scaling law ( $\tau_o^{\text{SC}}$ ), we get the time scale for critical slowing down of collective particle relaxation. The glass transition temperature ( $T_g$ ) is 68 K, which is below  $T_{p\text{-ZFC}} \sim 70$  K, suggesting that the glassy behavior of *superspins* closely follows the onset of blocking in the particles. This also explains the development of thermal hysteresis and its progressive enhancement below 68 K (Fig. 1). These results indicate that the nanoparticles show glassy behavior below  $T_g$  that may be SSG type and, below  $T_f \sim 48$  K, they collectively freeze.

To further elucidate these intriguing features, we performed memory effect in the FC aging protocol and the results are presented in Fig. 4(a). The sample was field cooled in an applied field of 50 Oe from 300 K to 5 K with intermittent stops (IS) at 90 K, 75 K, 50 K, 35 K, and 15 K. At each IS, the field was turned off for  $t_w = 10^4$  s and was turned back on during a further cooling process. This is shown by the  $M_{\text{FC-DN}}^{\text{IS}}$  curve. The sample then was warmed in a 50-Oe field from 5 K to 300 K without stopping shown by  $M_{\text{FC-UP}}^{\text{IS}}$ . The FCW curve is shown for reference. In the  $M_{\text{FC-DN}}^{\text{IS}}$  curve, a drop in magnetization is observed at every IS as the magnetic moments equilibrate; however, it is seen that the amount of drop depends on the magnetic state of the nanoparticles. After a waiting time  $t_w$ , when the field is turned on, the amount of recovery in magnetization ( $M$ ) depends on how fast the nanoparticles realign to the applied field. So, at temperatures below the  $T_g$  (50 K and 30 K), due to the critically slow dynamics of the

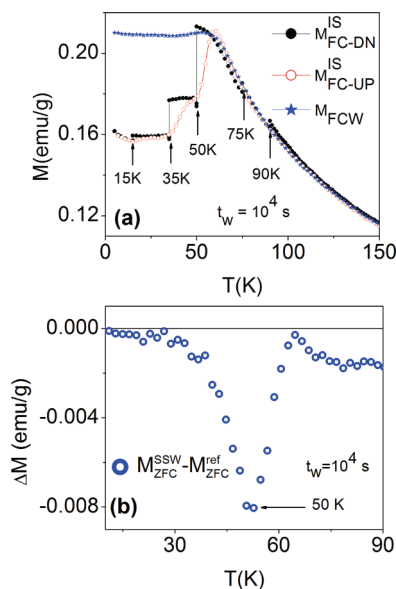


FIG. 4. (Color online) (a) Temperature dependence of  $M_{FC-DN}^{IS}$  and  $M_{FC-UP}^{IS}$  observed in the FC aging protocol and (b) temperature dependence of  $(M_{ZFC}^{SSW} - M_{ZFC}^{ref})$  in the ZFC aging protocol.

system, the recovery is less; hence, the observed drop in  $M$  is appreciable. It is to be noted here that at 15 K, the drop is relatively smaller. Also, there is an upturn in the  $M_{FC-DN}^{IS}$  curve below 15 K. Both these features can be attributed to the freezing of spins in the shell which is discussed later. Above  $T_g$  (90 K and 75 K), the nanoparticles do not show collective behavior and, hence, most of the drop in  $M$  is recovered when the field is turned on before further cooling. In the  $M_{FC-UP}^{IS}$  curve, it is seen that, on warming, the magnetization exhibits steplike features at every IS. Such a phenomenon has been observed in nanoparticles irrespective of their strength of interparticle interaction and is attributed to a distribution in energy barrier.<sup>32,33</sup> In the cooling process, at every IS, a certain amount of *dynamically active* nanoparticles with volume close to the blocking volume equilibrate and remain blocked on subsequent field cooling. So, at an IS during the cooling process, the magnetic moment configuration of the ensemble of nanoparticles is imprinted in its “memory.” This is retrieved in the warming process which results in the steplike feature in the  $M_{FC-UP}^{IS}$  curve.<sup>32</sup> We can conclude that the FC memory effect is more dominant below  $T_g$  when the dynamics of the nanoparticle ensemble critically slows down. In addition, the fact that the magnetization in field-cooled curves decreases with decreasing temperature suggests that the system is SSG like.

A peculiar test of SSG is the aging effect in the ZFC protocol, which is absent in the case of SPM particles.<sup>32</sup> In the single stop wait (SSW) protocol, the sample was cooled to 5 K under a zero field with an intermittent stop (IS) at 50 K for  $10^4$  s. The magnetization then was measured on warming ( $M_{ZFC}^{SSW}$ ) under an applied field of 50 Oe. The difference in magnetization ( $M_{ZFC}^{SSW} - M_{ZFC}^{ref}$ ) is plotted in Fig. 4(b), where  $M_{ZFC}^{ref}$  is the magnetization measured under the ZFC protocol without stopping. A peak in  $-(M_{ZFC}^{SSW} - M_{ZFC}^{ref})$  is seen at the IS temperature ( $\sim 50$  K) which is a signature of a SSG

system and its origin can be understood from the droplet model proposed by Fisher *et al.*<sup>34,35</sup> According to the droplet model, a spin-glass domain can be thought of as a droplet or a cluster whose volume increases with time because of the nonequilibrium nature of dynamics. In the SSW process as the droplet volume increases with time at 50 K, so does the mean energy barrier.<sup>34,35</sup> But, in the reference ZFC case, the energy barrier of the droplets at 50 K is relatively lower. During the warming process, it is known that the flip of clusters is governed by thermal activation. This means that  $M_{ZFC}^{ref}$  will be greater than  $M_{ZFC}^{SSW}$  at 50 K, because the *superspin* clusters associated with the reference ZFC cooling protocol are smaller and flip below 50 K, rendering higher magnetization than the bigger clusters formed in the SSW protocol that flip at higher temperature. This difference in magnetization at 50 K is seen as the peak in Fig. 4(b). It can be conclusively inferred that below  $T_g$ , the core-shell nanoparticles show aging and are of SSG type.

In view of our understanding of the system from the preliminary dc and ac magnetization results, two important inferences can be drawn: (i) the nanoparticles show cooperative behavior similar to SSG below  $T_g$  and (ii) there exist interparticle interactions in the SPM state that are dominant enough to maintain irreversibility in the ZFC-FCW curves, even at room temperature. So, as the temperature increases, the nanoparticles go from SSG to SPM state with finite interactions. In the case of granular thin films of FM nanoparticles embedded in a matrix, there have been studies indicating crossover from SSG to superferromagnet (SFM) with increasing concentration of FM nanoparticles.<sup>36</sup> It has also been demonstrated that for lower concentrations of FM nanoparticles, the SSG system goes into the interacting superparamagnet (ISPM) regime.<sup>37,38</sup> Now, the question that arises is as follows: At what temperature does the crossover from SSG to SPM occur in the present system? The answer to this is rather nontrivial. Usually an ensemble of nanoparticles is said to be in the SPM state above the blocking temperature identified as the temperature corresponding to the peak in the ZFC curve. This is true for monodisperse nanoparticles with negligible or no interactions. But, in the case of nanoparticles with finite-size distribution, there is always a precursor effect associated with unblocking of smaller particles at temperatures lower than  $T_{P-ZFC}$ . Moreover, the presence of interparticle interactions, and the formation of clusters further shift  $T_{P-ZFC}$  to higher temperature. In the case of core-shell nanoparticles, since the core and shell are composed of different materials, they have different magneto crystalline anisotropy, thermal activation, uncompensated spins, lattice strain, and so on. Hence, all these factors together suggest that  $T_{P-ZFC}$  may not be the true blocking temperature, at least in case of core-shell nanoparticles. We define the mean blocking temperature ( $\langle T_B \rangle$ ) as the temperature corresponding to the fastest change in the separation of ZFC from FCW curve, which, in turn, is associated with the maximum number of nanoparticles unblocking as the temperature increases.<sup>39</sup> This can be easily determined by identifying the peak position in  $\frac{d(M_{FCW} - M_{ZFC})}{dT}$ . Figure 5(a) shows the  $M(T)$  curves (left axis) measured at 100 Oe indicating the peak in ZFC curve ( $T_{P-ZFC}$ ), while on the right axis,  $-\frac{d(M_{FCW} - M_{ZFC})}{dT}$  is plotted against temperature whose peak marks  $\langle T_B \rangle$  as defined above.

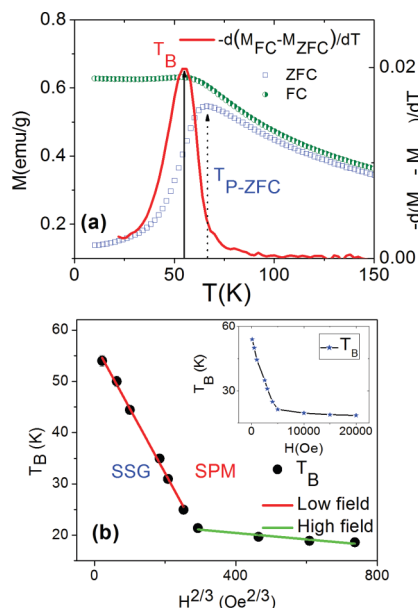


FIG. 5. (Color online) (a) ZFC/FC curve and the derivative  $d[M_{FC} - M_{ZFC}]/dT$  indicating peak temperature of  $M_{ZFC}$  ( $T_{pk}$ ) and mean blocking temperature ( $T_B$ ); (b) Two straight AT-line fits for low- and high-field regime. (Inset) The evolution of blocking temperature ( $T_B$ ) with measurement field.

In order to study the effect of applied field on  $\langle T_B \rangle$ ,  $M(T)$  measurements were conducted under the ZFC and FCW protocols in magnetic fields ranging from 50 Oe to 20 kOe. Generally, in the case of single domain particles, the blocking temperature monotonically shifts to lower temperatures due to lowering of the energy barrier on the application of magnetic field. Theoretically, the blocking temperature should decrease with the increasing applied field and eventually disappear when the field reaches a critical value; however, the rate of decrease in blocking temperature is strongly controlled by anisotropy,<sup>40</sup> dipole-dipole interaction,<sup>41</sup> and volume fraction of disordered spins. The inset of Fig. 5(b) shows the dependence of  $\langle T_B \rangle$  on an applied field. In the low-field regime,  $\langle T_B \rangle$  decreases sharply and, above  $\sim 6$  kOe, the decrease is gradual. The presence of two slopes suggests that the distribution of energy barrier is bimodal; one that is affected at low fields and another one at high fields. In the case of the core-shell nanoparticles, we have a single crystalline core and a shell composed of randomly oriented magnetic domains [Fig. 1(c)]. It has been reported that the effective anisotropy for hollow  $\gamma$ -Fe $_2$ O $_3$  is about  $\sim 8 \times 10^5$  J/m $^3$ , which is more than 5 times that of Fe nanoparticles<sup>42,43</sup> ( $\sim 1.3 \times 10^5$  J/m $^3$ ). This means that the mean energy barrier associated with the core ( $E_{cr}$ ) is lower than the one for the shell ( $E_{sh}$ ). The rate of decrease in  $\langle T_B \rangle$  is affected by the relative suppression of  $E_{cr}$  and  $E_{sh}$  in the low- and high-field regimes. In the low-field regime,  $E_{cr}$  is suppressed more while  $E_{sh}$  remains unaffected, which implies that the response of  $\langle T_B \rangle$  to field (sharp decrease) is predominantly influenced by the core. But, above a critical field, when the moments in the core are fully aligned, suppression of  $E_{sh}$  mainly contributes to the decrease in  $\langle T_B \rangle$ . In the case of nanoparticle systems, the presence of dipolar interactions has significant influence on the

magnetic properties as it modifies the anisotropy energy barrier of individual particles, thereby modifying the evolution of glassy dynamics<sup>44</sup> and blocking temperature.<sup>41</sup> The evolution of  $\langle T_B \rangle$  can be mapped on the H-T plane in order to distinguish the glassy phase from the SPM phase. From mean-field theory, it is predicted that the existence of glassy behavior for a fixed temperature will be destroyed above a critical field.<sup>30,45</sup> Two such critical lines were proposed by Almeida Thouless (AT line) and Gabay Thouless (GT line) for anisotropic Ising spins and for isotropic Heisenberg spins, respectively.<sup>45</sup> The AT line behaves as  $\langle T_B \rangle \propto H^{2/3}$ , while the GT line behaves as  $\langle T_B \rangle \propto H^2$ . Later it was shown by use of numerical calculations that such critical lines can exist in nanoparticles marking the transition from glassy to SPM behavior.<sup>46</sup> Figure 5(b) shows that the variation in  $\langle T_B \rangle$  follows the AT line in both the low-field and high-field regimes. Attempts to fit the GT line yielded straight lines in both low- and high-field regimes but with lower regression values compared to AT line. The fit is consistent with our calculations of  $z\nu$  from scaling law confirming that the system is indeed composed of Ising-type spins. We can infer that the nanoparticles behave like SSG to the left of the AT line and SPM to the right. The y intercept of the low-field regime fit is  $\sim 57$  K which can be attributed to the mean blocking temperature of the core at  $H = 0$  ( $T_{B1}$ ). Similarly, the y intercept of the high-field regime fit  $\sim 24$  K corresponds to the mean blocking temperature of the shell at  $H = 0$  ( $T_{B2}$ ). It has been reported in other systems that the critical behavior crosses over from AT line to GT line when the applied field is greater than the anisotropy field.<sup>47,48</sup> In the case of our core-shell nanoparticles, along with the presence of unidirectional random anisotropy, the exchange anisotropy is so high that such a crossover is not observed. This is supported by the fact that even at fields up to 20 kOe, irreversibility is observed between the ZFC and FCW curves.

From the above discussion, it is rather intriguing to estimate the temperature dependence of energy barrier. It was shown that the distribution in energy barrier can be mapped out from the temperature decay of remanence.<sup>49</sup> The remanent magnetization is related to the blocking temperature distribution function by Eq. (4).

$$I_r(T) = \alpha M_s \int_T^\infty f(T_B) dT_B. \quad (4)$$

Here,  $\alpha$  is a constant that takes into account the random orientation of anisotropy in the nanoparticles<sup>50</sup> and  $M_s$  is the saturation magnetization. The blocking temperature distribution function  $f(T_B)$  can be measured from the derivative of Eq. (4), i.e.,  $\frac{dI_r}{dT} \propto f(T_B)$ . The function  $f(T_B)$  represents the distribution of energy barrier. It is to be noted that the distribution function  $f(T_B)$  should not be confused with the mean blocking temperature  $\langle T_B \rangle$ . The measurement protocol was to expose the sample to a high field at a constant temperature; turn the field off and then measure the magnetization. Figure 6(a) shows the temperature dependence of remanent magnetization. As the temperature decreases, the remanent magnetization increases like in a conventional ferromagnet until  $\sim 35$  K, below which an unusual decrease is seen. The remanent magnetization is an indication of the number of moments that are still pointing along the direction of applied field after the field is removed. Below 35 K, the randomly

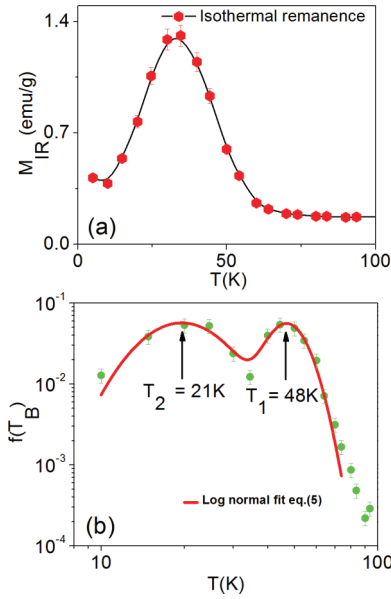


FIG. 6. (Color online) (a) Temperature dependence of isothermal remanence and (b) distribution function fit to Eq. (5).

oriented domains in the shell begin to show blocking behavior. Due to the random direction of blocking in the shell, the effective magnetization (at zero field) per nanoparticle drops which is seen as the drop in remanence. This is supported by the occurrence of a second peak ( $\sim 37$  K) in the ZFC curve at 2T due to blocking of shell (not shown). Figure 6(b) shows the temperature dependence of distribution  $f(T_B)$  or the energy barrier. The distribution  $f(T_B)$  is fitted to a weighted sum of two log normal distributions given by Eq. (5),

$$f(T_B) = \frac{A}{T_B \sqrt{2\pi} \sigma_1} \exp\left(-\frac{1}{2\sigma_1^2} \ln^2 \frac{T}{T_1}\right) + \frac{(1-A)}{T_B \sqrt{2\pi} \sigma_2} \exp\left(-\frac{1}{2\sigma_2^2} \ln^2 \frac{T}{T_2}\right). \quad (5)$$

The obtained fitted parameters are  $T_1 = 48$  K,  $\sigma_1 = 0.086$ ,  $T_2 = 21$  K,  $\sigma_2 = 0.33$  and the weighting factor  $A = 0.29$ . The existence of two maxima in the energy barrier is consistent with our findings from Fig. 5 and corroborates the fact that energy barriers  $E_{cr}$  and  $E_{sh}$  are centered about temperatures  $T_1$  and  $T_2$ , respectively. The maximum at  $T_1$  is at the same temperature as  $T_f$  obtained from ac susceptibility measurements. The low-field ac susceptibility measurement essentially probes the dynamics of the core since it has been discussed earlier that the disordered shell is affected only at high fields ( $>6$  kOe). So, one can say that the freezing temperature  $T_f \sim 48$  K as calculated from  $\chi'$  corresponds to the freezing of the core ( $T_{f-cr}$ ). Based on the same argument, the maximum at  $T_2$  ( $\sim 21$  K) can be attributed to the freezing of shell ( $T_{f-sh}$ ). This seems reliable since the freezing temperature  $T_{f-sh} \sim 21$  K is less than the mean blocking temperature of the shell ( $T_{B2} \sim 24$  K) calculated from the AT line fit [Fig. 5(b)]. Thus, we can identify two sets of mean blocking temperatures ( $T_{B1}$ ,  $T_{B2}$ ) and freezing temperatures ( $T_{f-cr}$ ,  $T_{f-sh}$ ) for the core and the shell, respectively.

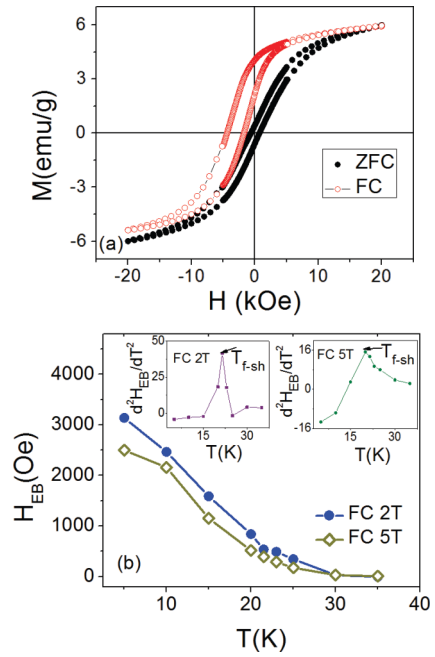


FIG. 7. (Color online) (a)  $M$ - $H$  hysteresis loops at 5 K under FC (2T) and ZFC conditions; (b) temperature dependence of exchange bias field measured for cooling magnetic fields of 2 T and 5 T. Insets show the  $\frac{d^2 H_{EB}}{dT^2}$  vs.  $T$  curves for cooling magnetic fields of 2T and 5T.

All the above experiments hint to the presence of EB and so we measured  $M(H)$  hysteresis loops at 5 K under the ZFC and FC (2T) protocol. Figure 7(a) shows the  $M(H)$  loops measured under ZFC and 2 T FC conditions. EB can be confirmed by the loop shift to the negative field axis as seen for the FC case. This is accompanied by an upward shift in the loop and enhanced coercivity, which has been observed in other EB systems.<sup>10,51-55</sup> The exchange bias field is calculated as  $H_{EB} = \frac{|(H^+ + H^-)|}{2}$ , where  $H^+$  and  $H^-$  are the coercive fields for the ascending and descending curves, respectively. In Fig. 7(b), the temperature dependence of EB field is plotted for cooling fields of 2 T and 5 T. One may argue that the onset temperature of exchange bias may depend on the magnetic field applied while cooling. So, we studied the temperature dependence of exchange bias for two different cooling fields (2 T and 5 T). In both cases, EB field starts to develop from  $\sim 35$  K and, as temperature decreases,  $H_{EB}$  increases slowly at first, followed by a rapid increase. In the insets [Fig. 7(b)], we have plotted the rate of change of  $\frac{dH_{EB}}{dT}$  with respect to temperature, in other words,  $\frac{d^2 H_{EB}}{dT^2}$  vs. temperature, whose peak corresponds to the temperature below which EB exhibits a rapid rise. This rapid rise in EB was found to occur at 21.5 K and 20 K for cooling fields of 2 T and 5 T, respectively, which are in proximity to  $T_{f-sh}$  ( $\sim 21$  K). From our previous discussion, at 35 K, the core is frozen with its spins aligned along the field and the shell begins to show a blocking behavior. Due to the slow dynamics of the blocked spins ( $<35$  K) in the shell they behave as pinning centers leading to the development of EB. This marks the onset of EB in the core-shell nanoparticles. Below 21 K ( $<T_{f-sh}$ ), when the shell is completely frozen, the number of pinning centers increase due to enhanced exchange

coupling between the core and the shell. Although the strength of the exchange coupling constant of each exchange coupled bond remains constant, this phenomenon can be attributed to the increase in density of exchange coupled bonds across the core-shell interface (i.e., number of frozen spins at the interface per unit area) and is consistent with results from previous studies.<sup>4,56–58</sup> In our discussion on the magnetic state of the core and the shell, the term *frozen* is used with respect to time scale, i.e., the collective reversal mechanism of moments in the ground state (absence of external magnetic field) occurs over a large time span (several hundred seconds). For a system to display exchange bias, there must exist at least two exchange coupled phases: one reversible phase that can be reversed and one fixed phase that cannot be reversed in the field range of measurements.<sup>3,7</sup> In the context of our core-shell nanoparticles, the fixed phase is the “shell” and the reversible phase is the “core.” At low temperatures below  $\sim 35$  K, while the shell behaves as the fixed phase, the magnetization of the “frozen” core can be reversed by application of an external field. The reversal of the core moments with respect to the shell moments leads to exchange bias, which has been reported in previous studies. Below  $\sim 21$  K, a rapid increase in EB is observed [Fig. 7(b)], which can be explained by the same mechanism as discussed above. The enhancement in EB occurs due to an increase in the number of frozen spins at the interface per unit area,<sup>56</sup> which has been argued to develop due to freezing of the shell moments. Consistently, a rapid increase in  $H_{EB}$  is recorded below  $T_{f-sh}$ . So, one can conclude that in the case of core-shell nanoparticles, the onset of EB is associated with the blocking of spins in the shell while the core is in the frozen state.

#### IV. CONCLUSIONS

In summary, we have investigated the static and dynamic magnetic behavior of Fe/ $\gamma$ -Fe<sub>2</sub>O<sub>3</sub> core-shell nanoparticles. The nanoparticles exhibit a collective SSG-type behavior below the glass transition temperature and show signs of aging. We demonstrate that the response of the core-shell nanoparticles in different low/high magnetic field regimes is different and greatly influences the mean blocking temperature. The core responds to low fields while the shell is unaffected; however, at high fields, when the core is saturated,  $\langle T_B \rangle$  is influenced by the dynamics of the shell. The energy barrier distribution is found to have two maxima corresponding to the individual freezing of the core and shell. Finally, we have shown conclusive evidence that the onset of EB depends on the magnetic state of the core and shell. EB is found to develop at the temperature that marks the onset of shell blocking below the freezing temperature of the core. These observations opens up the possibility of tailoring EB and its onset temperature by suitably choosing different materials for the core and shell that show blocking and freezing phenomena at a desired temperature range.

#### ACKNOWLEDGMENTS

The research was supported by the DOE through Grant No. DE-FG02-07ER46438. H.S. also acknowledges support from the Center for Integrated Functional Materials through Grant No. USAMRMC W81XWH-10-2-0101. M.H.P. thanks the support from the Florida Cluster for Advanced Smart Sensor Technologies.

- 
- <sup>1</sup>R. L. Stamps, *J. Phys. D: Appl. Phys.* **33**, R247 (2000).  
<sup>2</sup>M. Kiwi, *J. Magn. Magn. Mater.* **234**, 584 (2001).  
<sup>3</sup>J. Nogues and I. K. Schuller, *J. Magn. Magn. Mater.* **192**, 203 (1999).  
<sup>4</sup>O. Iglesias, A. Labarta, and X. Batlle, *J. Nanosci. Nanotechnol.* **8**, 2761 (2008).  
<sup>5</sup>S. Giri, M. Patra, and S. Majumdar, *J. Phys. Condens. Matter* **23**, 073201 (2011).  
<sup>6</sup>S. Laureti, S. Y. Suck, H. Haas, E. Prestat, O. Bourgeois, and D. Givord, *Phys. Rev. Lett.* **108**, 077205 (2012).  
<sup>7</sup>W. H. Meiklejohn and C. P. Bean, *Phys. Rev.* **105**, 904 (1957).  
<sup>8</sup>A. Maitre, D. Ledue, and R. Patte, *J. Magn. Magn. Mater.* **324**, 403 (2012).  
<sup>9</sup>K. Nadeem, H. Krenn, T. Traussing, and I. Letofsky-Papst, *J. Appl. Phys.* **109**, 013912 (2011).  
<sup>10</sup>S. Karmakar, S. Taran, E. Bose, B. K. Chaudhuri, C. P. Sun, C. L. Huang, and H. D. Yang, *Phys. Rev. B* **77**, 144409 (2008).  
<sup>11</sup>M. Xu, W. Zhong, J. Yu, W. Zang, C. Au, Z. Yang, L. Lv, and Y. Du, *J. Phys. Chem. C* **114**, 16143 (2010).  
<sup>12</sup>M. Ali, P. Adie, C. H. Marrows, D. Greig, B. J. Hickey, and R. L. Stamps, *Nat. Mater.* **6**, 70 (2007).  
<sup>13</sup>F.-T. Yuan, J.-K. Lin, Y. D. Yao, and S.-F. Lee, *Appl. Phys. Lett.* **96**, 162502 (2010).  
<sup>14</sup>M. Gruyters, *Eur. Phys. Lett.* **77**, 57006 (2007).  
<sup>15</sup>Q. K. Ong, A. Wei, and X.-M. Lin, *Phys. Rev. B* **80**, 134418 (2009).  
<sup>16</sup>X. Sun, N. F. Huls, A. Sigdel, and S. Sun, *Nano Lett.* **12**, 246 (2012).  
<sup>17</sup>Y. Hu and A. Du, *J. Appl. Phys.* **110**, 1967 (2011).  
<sup>18</sup>H. Khurshid, V. Tzitzios, W. Li, C. G. Hadjipanayis, and G. C. Hadjipanayis, *J. Appl. Phys.* **107**, 09A333 (2010).  
<sup>19</sup>A. Cabot, A. P. Alivisatos, V. F. Puentes, L. Balcells, O. Iglesias, and A. Labarta, *Phys. Rev. B* **79**, 094419 (2009).  
<sup>20</sup>M. Suzuki, S. I. Fullem, I. S. Suzuki, L. Wang, and C.-J. Zhong, *Phys. Rev. B* **79**, 024418 (2009).  
<sup>21</sup>C. R. Lin, R. K. Chiang, J. S. Wang, and T. W. Sung, *J. Appl. Phys.* **99**, 08N710 (2006).  
<sup>22</sup>L. He, *Solid State Commun.* **150**, 743 (2010).  
<sup>23</sup>J. L. Dormann, D. Fiorani, and E. Tronc, *J. Magn. Magn. Mater.* **202**, 251 (1999).  
<sup>24</sup>S. Pal, S. Chandra, M.-H. Phan, P. Mukherjee, and H. Srikanth, *Nanotechnology* **20**, 485604 (2009).  
<sup>25</sup>J. D. Moore, G. K. Perkins, K. Morrison, L. Ghivelder, M. K. Chattopadhyay, S. B. Roy, P. Chaddah Jr., A. K. Gschneidner, V. K. Pecharsky, and L. F. Cohen, *J. Phys. Condens. Matter* **20**, 465212 (2008).  
<sup>26</sup>G. P. Zheng and J. X. Zhang, *J. Phys. Condens. Matter* **10**, 275 (1998).  
<sup>27</sup>K. De, S. Majumdar, and S. Giri, *J. Appl. Phys.* **101**, 103909 (2007).

- <sup>28</sup>J. A. Mydosh, *Spin Glasses: An Experimental Introduction* (Taylor & Francis, London, 1993).
- <sup>29</sup>X. Chen, S. Bedanta, O. Petravic, W. Kleemann, S. Sahoo, S. Cardoso, and P. P. Freitas, *Phys. Rev. B* **72**, 214436 (2005).
- <sup>30</sup>K. Binder and A. P. Young, *Phys. Rev. B* **29**, 2864 (1984).
- <sup>31</sup>C. Djurberg, P. Svedlindh, P. Nordblad, M. F. Hansen, F. Bodker, and S. Morup, *Phys. Rev. Lett.* **79**, 5154 (1997).
- <sup>32</sup>M. Sasaki, P. E. Jonsson, H. Takayama, and H. Mamiya, *Phys. Rev. B* **71**, 104405 (2005).
- <sup>33</sup>R. K. Zheng, H. W. Gu, and X. X. Zhang, *Phys. Rev. Lett.* **93**, 139702 (2004).
- <sup>34</sup>D. S. Fisher and D. A. Huse, *Phys. Rev. B* **38**, 386 (1988).
- <sup>35</sup>D. S. Fisher and D. A. Huse, *Phys. Rev. B* **38**, 373 (1988).
- <sup>36</sup>J. Alonso, M. L. Fdez-Gubieda, J. M. Barandiaran, A. Svalov, L. Fernandez Barquin, D. Alba Venero, and I. Orue, *Phys. Rev. B* **82**, 054406 (2010).
- <sup>37</sup>H. M. Nguyen, D. H. Manh, L. V. Hong, N. X. Phuc, and Y. D. Yao, *J. Korean Phys. Soc.* **52**, 1447 (2008).
- <sup>38</sup>P. Allia, M. Coisson, P. Tiberto, F. Vinai, M. Knobel, M. A. Novak, and W. C. Nunes, *Phys. Rev. B* **64**, 144420 (2001).
- <sup>39</sup>J. C. Denardin, A. L. Brandl, M. Knobel, P. Panissod, A. B. Pakhomov, H. Liu, and X. X. Zhang, *Phys. Rev. B* **65**, 064422 (2002).
- <sup>40</sup>X. X. Zhang, H. L. Wei, Z. Q. Zhang, and L. Y. Zhang, *Phys. Rev. Lett.* **87**, 157203 (2001).
- <sup>41</sup>S. Morup and E. Tronc, *Phys. Rev. Lett.* **72**, 3278 (1994).
- <sup>42</sup>H. Khurshid, W. Li, V. Tzitzios, and G. C. Hadjipanayis, *Nanotechnology* **22**, 265605 (2011).
- <sup>43</sup>B. Mehdaoui, A. Meffre, L. M. Lacroix, J. Carrey, S. Lachaize, M. Respaud, M. Gougeon, and B. Chaudret, *J. Appl. Phys.* **107**, 09A324 (2010).
- <sup>44</sup>T. Jonsson, J. Mattsson, C. Djurberg, F. A. Khan, P. Nordblad, and P. Svedlindh, *Phys. Rev. Lett.* **75**, 4138 (1995).
- <sup>45</sup>K. Binder and A. P. Young, *Rev. Mod. Phys.* **58**, 801 (1986).
- <sup>46</sup>L. E. Wenger and J. A. Mydosh, *Phys. Rev. B* **29**, 4156 (1984).
- <sup>47</sup>G. Kotliar and H. Sompolinsky, *Phys. Rev. Lett.* **53**, 1751 (1984).
- <sup>48</sup>N. deCourtenay, A. Fert, and I. A. Campbell, *Phys. Rev. B* **30**, 6791 (1984).
- <sup>49</sup>R. W. Chantrell, M. Elhilo, and K. Ogrady, *IEEE Trans. Magn.* **27**, 3570 (1991).
- <sup>50</sup>C. P. Bean, J. D. Livingston, and D. S. Rodbell, *J. Phys. Radium* **20**, 298 (1959).
- <sup>51</sup>H. M. Nguyen, P.-Y. Hsiao, and M.-H. Phan, *J. Appl. Phys.* **107**, 09D706 (2010).
- <sup>52</sup>K. Nadeem and H. Krenn, *J. Supercond. Novel Magn.* **24**, 717 (2011).
- <sup>53</sup>B. Martinez, X. Obradors, L. Balcells, A. Rouanet, and C. Monty, *Phys. Rev. Lett.* **80**, 181 (1998).
- <sup>54</sup>T. N. Shendruk, R. D. Desautels, B. W. Southern, and J. van Lierop, *Nanotechnology* **18**, 455704 (2007).
- <sup>55</sup>R. K. Zheng, G. H. Wen, K. K. Fung, and X. X. Zhang, *Phys. Rev. B* **69**, 214431 (2004).
- <sup>56</sup>Q. K. Ong, X.-M. Lin, and A. Wei, *J. Phys. Chem. C* **115**, 2665 (2011).
- <sup>57</sup>O. Iglesias, X. Batlle, and A. Labarta, *Phys. Rev. B* **72**, 212401 (2005).
- <sup>58</sup>E. Eftaxias and K. N. Trohidou, *Phys. Rev. B* **71**, 134406 (2005).